Cardiovasc Intervent Radiol (2019) 42:1466–1474
https://doi.org/10.1007/s00270-019-02241-6

Sequential and Simultaneous 4-Antenna Microwave Ablation in an Ex Vivo Bovine Liver Model

Tian-qi Zhang[1] · Sen-miao Huang[2] · Yang-kui Gu[1] · Xiong-ying Jiang[3] · Zhi-mei Huang[1] · Han-xia Deng[1] · Jin-hua Huang[1]

Published online: 20 May 2019

Abstract

Aims To determine the sizes and shapes of ablation zones in 4-antenna microwave ablation in ex vivo bovine liver model under different conditions of power delivery patterns, antenna spacings, and ablation durations, for further using of multi-antenna MWA strategies in the treatment of large hepatocellular carcinoma.

Methods We tested protocols of eight ablations each on ex vivo bovine livers, involving simultaneous or sequential activation of four microwave antennas, spaced either 3 cm, 4 cm, or 5 cm apart, for either 10 or 15 min, at 60-W power. We determined the diameters, shapes, and temperatures of the ablation zones.

Results Compared to sequential power delivery, simultaneous power delivery resulted in significantly larger ablation zone diameters ($P < .001$). The temperatures in ablation zones were significantly higher for simultaneous than for sequential power delivery. The largest ablation diameter (7.45 ± 0.06 cm) resulted from simultaneous delivery for 15 min using 4-cm antenna spacing.

Conclusions Simultaneous 4-antenna microwave ablation results in larger ablation zones than sequential ablation, and 4-cm antenna spacing with a 15-minute ablation duration creates the largest ablation zone. This information may provide multi-antenna MWA strategies for large HCC in the further clinical practice.

Keywords Microwave · Ablation · Sequential · Simultaneous · 3D reconstruction

Introduction

It has been reported that 70% of patients with hepatocellular carcinoma (HCC) suffer from large tumors, most of which are not suitable for surgical resection, for reasons that may include poor hepatic function reserve and complex anatomic location [1–3]. Image-guided microwave ablation (MWA) has been considered a viable alternative for treating small HCC less than 3 cm [4]. However, because many large HCC have diameters greater than that, an overlapping method is required for MWA to be useful [5].

Overlapping monopolar radiofrequency ablation (RFA) has been used to treat large hepatic tumors. However, overlapping methods presented technical challenges, and patients remained at risk for tumor residual or progression

Electronic supplementary material The online version of this article (https://doi.org/10.1007/s00270-019-02241-6) contains supplementary material, which is available to authorized users.

Tian-qi Zhang and Sen-miao Huang contributed equally to this work and are considered co-first authors.

✉ Jin-hua Huang
huangjh@sysucc.org.cn

[1] Department of Minimally Invasive Interventional Radiology, State Key Laboratory of Oncology in South China, Collaborative Innovation Center for Cancer Medicine, Sun Yat-sen University Cancer Center, 651 Dongfeng East Road, Guangzhou 510060, People's Republic of China

[2] Department of Oncology, Panyu Central Hospital, 8 Fuyu East Road, Guangzhou 511400, People's Republic of China

[3] Department of Interventional Radiology, Sun Yat-sen Memorial Hospital, Sun Yat-sen University, 107 Yanjiang West Road, Guangzhou 510120, People's Republic of China

as the tumors were larger than 6 cm in diameter [6]. It has been reported that up to three RF electrodes could be applied simultaneously to expand the ablation zone by a confluent thermal field compared to single-electrode RFA [7]. However, there is still only one-circuit radiofrequency electrical current generated by one RF generator in multi-electrode RFA, with this one-circuit current either switched one-by-one among each electrode sequentially by a switch-controller RF generator or simply shared equally to each electrodes [8–10]. Conversely, microwave energy can be applied simultaneously via multiple antennas, with each antenna generated by each MW generator separately, which some have suggested may create a more confluent and larger heating zone [11–15].

Simultaneous MWA with multiple antennas applied to liver models has resulted in larger ablation zones when compared to sequential MWA [5, 11]. However, these studies were carried out using relatively low power, narrow antenna spacing, and short ablation durations, with three or fewer antennas. We are not aware of any studies using 4-antenna MWA in liver models.

Our objective was to determine the sizes and shapes of ablation zones in 4-antenna MWA under different conditions in ex vivo bovine liver. The results might provide multi-antenna MWA strategies for large HCC in the further clinical practice.

Materials and Methods

We used 43 ex vivo bovine livers (weight range, 5.1–6.3 kg), which were harvested at a local slaughterhouse and kept at approximately 25 °C, and we performed two or three ablations in each liver.

Equipment

The VISON-GEN microwave generator (Vison-China Medical Devices R&D Center, Nanjing, P. R. China), which provided a microwave frequency of 2450 MHz and a single output channel, was used in this study. The VISON-GEN provided constant power to each MW antenna solely, a single-use coaxial interstitial microwave antenna measuring 14G in diameter and 18 cm in length (VISON-PROBE, Vison-China Medical Devices), coupled with a peristaltic VISON-PUMP for convective antenna cooling.

Ablation Protocols

We performed eight ablations using each of the 12 ablation protocols (Fig. 1). We tested six simultaneous activation protocols, which were all activated at the same time for either 10 or 15 min, and another six sequential activation protocols, which were each activated in succession for the total ablation times either 40 or 60 min, both involving four microwave antennas, which were spaced either 3 cm, 4 cm, or 5 cm apart, and with setting power for each antenna at 60 W.

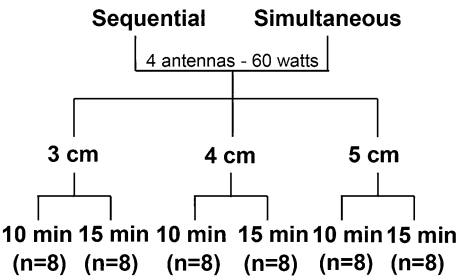

Fig. 1 Experimental design comparing sequential and simultaneous 4-antenna microwave ablations in ex vivo bovine livers. Experimental design includes six protocols involving sequential activation, and 6 protocols involving simultaneous activation, all using four microwave antennas, which were spaced either 3 cm, 4 cm, or 5 cm apart, and each antenna activated with 60 Watts power for either 10 or 15 min

Temperature Monitoring

For each ablation, five temperature sensors with 1-cm spacing were placed, labeled A through E, in a straight radial line which bisected an axis of symmetry through the four antennas, beginning at the center of the antenna array and extending toward the periphery (Fig. 2). A customized acrylic plate was used to ensure precision of needles placement. The temperatures from each sensor in both simultaneous and sequential activation of the four antennas were recorded every minute for the ablation durations of 15 min and cooling periods of 10 min (Fig. 2). Then the mean maximum temperatures recorded by each sensor for each protocol were calculated.

3D Reconstruction Visualization of the Ablation Zone

To determine the volume and shape of the ablation zone, a 3D visualization system (Hokai Medical Devices co., Ltd., Zhuhai, China), which allowed segmentation and 3D reconstruction of the Magnetic resonance (MR) images in DICOM format, was applied in this study before the ablated ex vivo bovine livers were dissected. All local MR images were acquired with 3.0-T MR imaging systems (Magnetom Verio or Trio TIM, Siemens Healthcare, or Discovery MR 750, GE). As the coagulation necrosis zone in ex vivo livers were well distinguishing on T2-weighted images, then we acquired only the T2-weighted images, which were obtained with repetition time 2137–5360 ms; echo time 60–119 ms; section thickness 3.0 mm. The

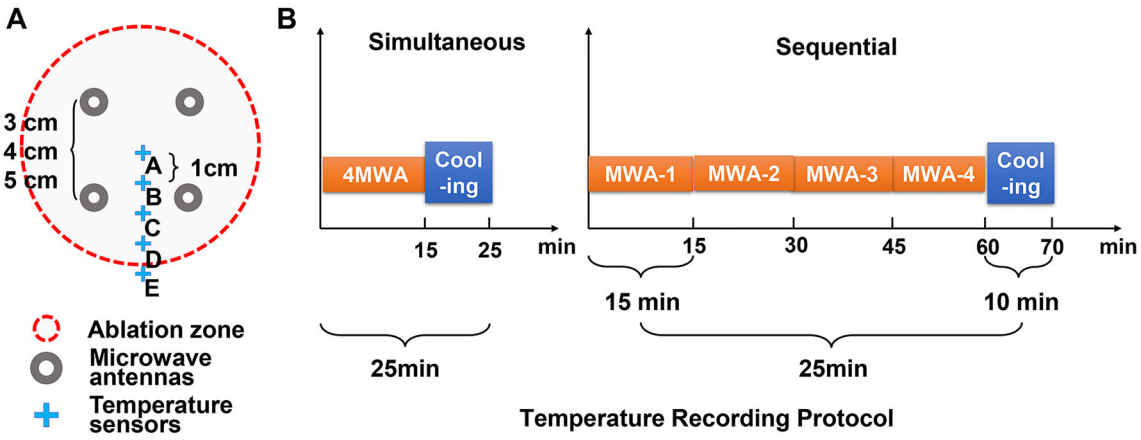

Fig. 2 Positioning of microwave antennas and temperature sensors (**A**) and temperature recording protocols (**B**) during 4-antenna microwave ablation in ex vivo bovine livers. **A** Four microwave antennas (O) were placed either 3 cm, 4 cm, or 5 cm apart, and five temperature sensors (+) were placed in a straight radial line which bisected an axis of symmetry through the four antennas, so that sensor A was positioned at the center of the antenna array and sensors B–E were positioned in sequence every 1 cm along the radial line. **B** Duration of temperature recording during simultaneous microwave ablation using four antennas (4MWA) and sequential microwave ablation using four antennas (MWA-1, MWA-2, MWA-3, MWA-4), both with ablation durations of 15 min (min) and cooling periods of 10 min; for both ablation protocols, total duration of temperature recording was 25 min

ablation zone and the bovine liver were segmented rapidly and displayed intuitional in the 3D visualization system, based on the series of MRI data (3-mm-thick slices) of the ablated liver in DICOM format. As soon as the segmentation was completed, the volume of the ablation zone was calculated by the 3D reconstruction software (Hokai Medical Devices co., Ltd., Zhuhai, China) automatically.

Ablation Zone Measurements and Ratios

The livers then were sliced transversely across the antenna insertion track, in approximately 5-mm-thick increments, and the central slice of each ablation zone was stored as a digital image. The ImageJ (v1.39e, National Institutes of Health, Bethesda, MD, USA) was used for tissue measurements. Two investigators measured the ablation zone diameters and the post-ablation antenna spacing distances and recorded the average.

Because the descriptions of the shape of each ablation zone were subjective and hard to define, we developed the cleft ratio (*CR*) as a way to quantify defects within the ablation zones and define ablation shapes more objectively. The *CR* was calculated using the formula:

$$CR = \frac{D - d}{D}$$

where circumscribed diameter (D) and inscribed diameter (d) were measured as the diameter of the smallest or largest possible circle that could be drawn around or inside the ablation zone. The shapes of the ablation zones in this study could be divided into four types based on the characteristics (Fig. 3): (1) confluent, in which the ablation zone was similar to a circle, with a *CR* between 0 and 0.15; (2) margin cleft, in which concave clefts appeared at the ablation zone margins, with a *CR* ranging from > 0.15 to 0.59; (3) central cleft, in which concave clefts appeared at both the ablation zone margins and centers, with a *CR* ranging from > 0.59 to < 1.0; and (4) divergent, in which even more prominent concave clefts appeared at the ablation zone margins and centers, creating four separate small ablation zones, with a *CR* of 1.0.

The spherical ratio was calculated by the isoperimetric quotient: $(4 \times \pi \times \text{area})/\text{perimeter}^2$. The contraction ratio was applied to describe the extent of tissue shrinkage after ablation, calculated as: $1 - (\text{antenna spacing}_{\text{after}}/\text{antenna spacing}_{\text{before}})$ [16], where antenna $\text{spacing}_{\text{after}}$ was the average measurement of the spacings between the four antennas after ablation.

Statistical Methods

For each 8-ablation protocol, mean values and standard deviations (SD) for each parameter and ratio were calculated. The linear mixed-effects models with SPSS software (Version 25.0, SPSS Inc., Chicago, IL, USA) was applied to analyze the data. In these models, fixed-effect variables included pattern of power delivery, antenna spacing, and ablation duration; response variables included ablation zone circumscribed diameter, inscribed diameter, *CR*, spherical ratio, and contraction ratio. Significant differences between the groups were determined using LSD test. The statistical significance was defined at the 5% ($P < .05$) level.

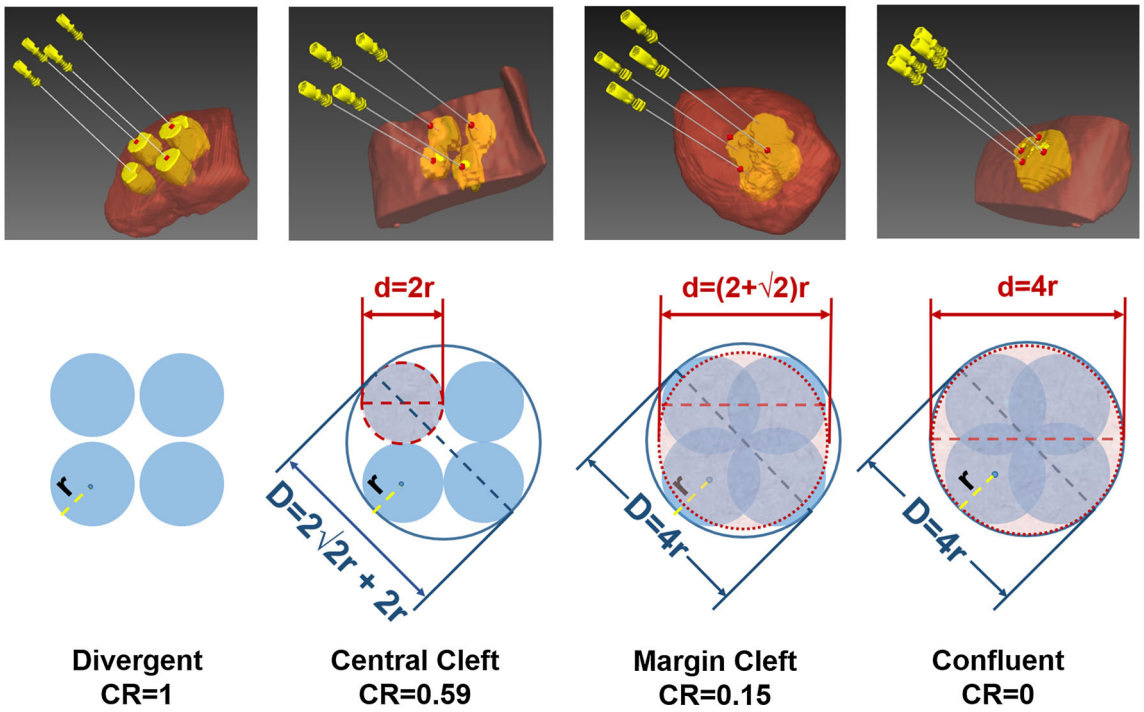

Fig. 3 Diagrams of four ablation zone shapes with the 3D reconstruction visualization and cleft ratios identified after 4-antenna microwave ablation in ex vivo bovine livers. Examples of the four ablation zone shapes identified during 4-antenna microwave ablation are represented here: divergent, central cleft, margin cleft, and confluent, respectively. The cleft ratio (*CR*) ranges from 1 to 0 and is calculated using the formula: $(D - d)/D$, where D is the circumscribed diameter (diameter of smallest possible circle that can be drawn around the polygonal ablation zone, passing through all the vertices of the polygon), and d is the inscribed diameter (diameter of largest possible circle that can be drawn inside the polygonal ablation zone, with circle tangent to each side of the polygon.). A smaller *CR* suggests smaller clefts, or untreated portions, within the ablation zone. In the diagrams, "*r*" represents the radius of the ablation zone around a single microwave antenna

Results

Changing Antenna Spacing

For the simultaneous ablation protocol using 15-minute ablation duration, as the spacing between antennas increased, the inscribed diameter initially increased (from 6.95 ± 0.31 cm at 3-cm spacing to 7.45 ± 0.06 cm at 4-cm spacing), and then decreased (to 6.57 ± 0.16 cm at 5-cm spacing) (Fig. 4, Supplementary Table 1). For the same protocol, as the antenna spacing increased, the *CR* also increased (from 0.09 ± 0.04 at 3 cm, to 0.15 ± 0.02 at 4 cm, to 0.36 ± 0.02 at 5 cm), the ablation zone shape changed from confluent to margin cleft, and the spherical ratio decreased (from 0.98 ± 0.01 at 3 cm, to 0.94 ± 0.01 at 4 cm, to 0.74 ± 0.01 at 5 cm).

Changing Power Delivery Pattern

For the ablation protocols using antennas spaced 3 cm apart, simultaneous power delivery resulted in larger inscribed diameters than sequential delivery at both 10-minute and 15-minute ablation durations. Similarly, for 4-cm antenna spacing, simultaneous delivery resulted in larger volumes than sequential delivery at both 10-minute and 15-minute (274.56 ± 17.34 cm^3 vs. 254.48 ± 15.67 cm^3) ablation durations (Supplementary Table 1). However, for 5-cm antenna spacing, power delivery pattern did not affect the volume of the ablation zone at 10-minute duration.

Changing Ablation Duration

For the sequential ablation protocol at 5-cm antenna spacing, as the duration increased from 10 to 15 min, the volume significantly increased (from 175.62 ± 9.28 to 226.80 ± 20.63 cm^3) (Supplementary Table 1). In the linear mixed-effects model, longer ablation duration resulted in significantly larger mean inscribed diameters, volumes, and spherical ratios ($P < .001$ for both) (Table 1).

Cleft Ratios

In the linear-effects model, the mean *CR* was significantly lower for simultaneous than sequential power delivery

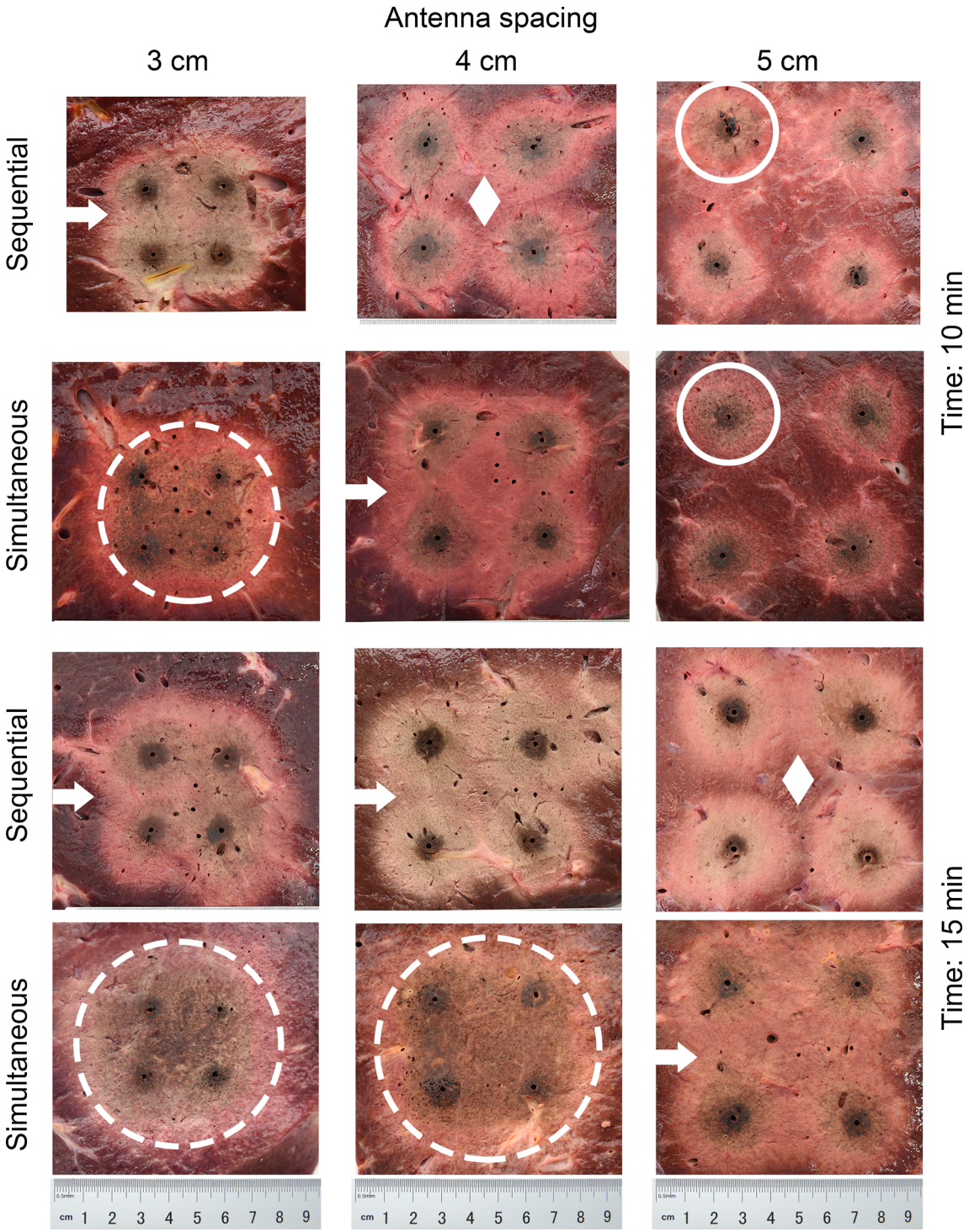

Fig. 4 Photographic images of 4-antenna microwave ablation zones in ex vivo bovine livers using different power delivery patterns, antenna spacings, and ablation durations. Representative images illustrate different ablation zone shapes resulting from differing power delivery patterns (sequential or simultaneous), 4-antenna spacings (3 cm, 4 cm, or 5 cm), and ablation durations (10 min or 15 min). The four ablation zone shapes identified were confluent (broken circle), margin cleft (bold arrow, →), central cleft (bold rhombus, ◇), and divergent (solid circle, ○). Ablation zone-inscribed diameters (double arrow broken line, ↔) varied in length; the largest was created by simultaneous microwave ablation with 4-cm antenna spacing and 15-minute treatment duration, and it measured 7.45 ± 0.06 cm

Table 1 Statistical significance results (*P* values) for differences among response variables for different fixed-effect variables, after 4-antenna microwave ablation in ex vivo bovine livers

Fixed effects		Response variables					
Type	Variable	Diameter		Volume	Cleft ratio	Spherical ratio	Contraction ratio
		Circumscribed	Inscribed				
Power delivery pattern	Sequential versus simultaneous[2]	.09	< .001	< .001	< .001	< .001	< .001
Ablation duration	10 min versus 15 min	.18	< .001	< .001	< .001	< .001	< .001
Antenna spacing	3 cm versus 4 cm	< .001	< .001	< .001	< .001	< .001	< .001
	4 cm versus 5 cm	< .001	< .001	< .001	< .001	< .001	< .001
	3 cm versus 5 cm	< .001	< .001	0.03	< .001	< .001	< .001

cm centimeters, *min* minutes

pattern ($P < .001$), for 3-cm than 4-cm ($P < .001$) and 5-cm ($P < .001$) antenna spacings, and for 15-minute than 10-minute ablation duration ($P < .001$) (Table 1).

Contraction Ratios

The mean contraction ratio was significantly higher for simultaneous than sequential power delivery pattern ($P < .001$), for 3-cm and 4-cm than 5-cm antenna spacings (both $P < .001$), and for 15 min than 10 min ablation duration ($P < .001$) (Table 1), with the highest contraction ratio being 0.20 ± 0.03 with simultaneous ablation and 3-cm antenna spacing for 15 min.

Ablation Zone Temperatures

The mean maximum temperatures recorded by sensors A through E were all significantly higher for simultaneous power delivery than for sequential power delivery ($P < .001$) (Fig. 5). And at any given power delivery pattern and ablation duration, the mean maximum temperatures were lower as the antenna spacing increased. Also, the mean maximum temperatures recorded by the most peripheral sensors, D and E, respectively, were higher for 4-cm antenna spacing (79 °C and 58 °C) than for either 3-cm (75 °C and 55 °C) or 5-cm (59 °C and 50 °C) spacings.

Discussion

Treatment of large HCC with conventional MWA using multiple overlapping antennas may present technical challenges, potentially resulting in insufficient tumor ablation, tumor residual, and recurrence or progression. In this study, we have determined the shapes and diameters of 4-antenna MWA zones in an ex vivo bovine liver model. As the other studies reported, by applying microwave ablation to induce a broader ablation zone can lead to a real survival benefit, even for perivascular HCC [17–19]. Our findings may provide helpful insights into the use of multi-antenna MWA for large HCC in humans.

We identified four different ablation zone shapes, which we named confluent, margin cleft, central cleft, and divergent, based on the observations in the previous unpublished multi-antenna MWA work, in which V-shaped ablation zone defects, or clefts, were visible in various combinations at the margins and centers of the ablation zones. The specific *CR* ranges were proved to correspond with each of the four shapes. Furthermore, three-dimensional reconstruction models facilitate acquisition of intuitionistic and omnidirectional information about the ablation zones and the normal liver tissue. More importantly, 3D reconstruction has advantages in evaluating the volumes of the ablation zone more accurately than the measurement based on 2D dissected surface [20]. Therefore, 3D reconstruction can improve accuracy and intuitiveness to determine the shape and volume. We were unable to find any previous numerical descriptions of 4-antenna ablation zone shapes in the literature, and we propose that *CR* may be a useful tool for quantifying and comparing the shapes of 4-antenna MWA zones.

As to the influence of antenna spacing, Oshima et al. have reported the effect of different antenna spacings in MWA and noted that the largest ablation zone (4.2 cm diameter) was obtained with 2-cm antenna spacing [12]. Besides, there were a number of reports focusing on different probe spacings including irreversible electroporation [21] and bipolar radiofrequency ablation (RFA) [22]. Mulier et al. used four bipolar RFA electrodes and found that the largest ablation zones were created also with 2-cm electrode spacing [23]. These findings point out that RFA energy does not continue to disperse through charred

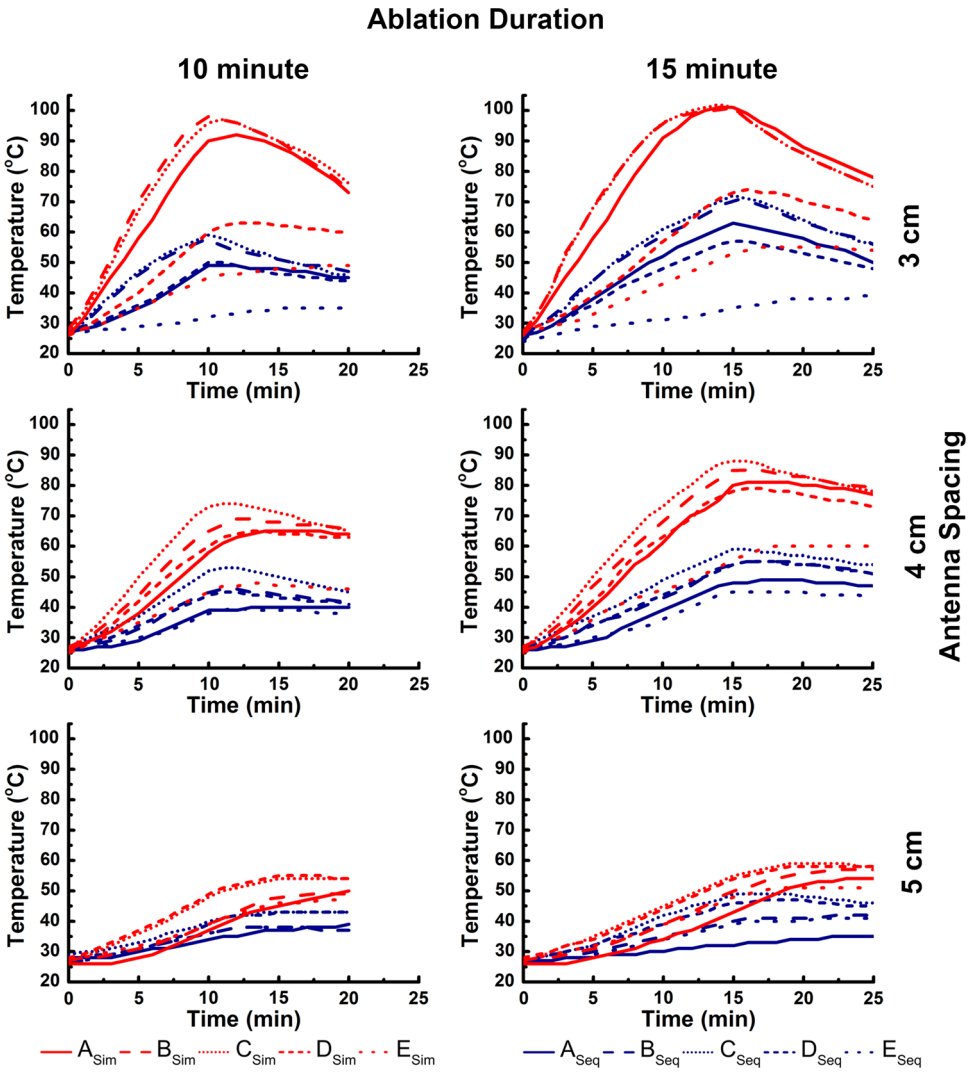

Fig. 5 Mean temperature variations during 4-antenna microwave ablation in ex vivo bovine livers recorded by five temperature sensors and using different power delivery patterns, antenna spacings, and ablation durations. Graphs showing mean temperature variations recorded by five different temperature sensors (A–E) during 4-antenna microwave liver ablation, resulting from differing ablation durations (10 min or 15 min), antenna spacings (3 cm, 4 cm, or 5 cm), and power delivery patterns (sequential [Seq] or simultaneous [Sim]). At any given antenna spacing and ablation duration, the mean maximum temperatures were higher for simultaneous than sequential ablation. At any given power delivery pattern and antenna spacing, the mean maximum temperatures were higher for 15-minute than for 10-minute ablation durations. However, depending upon the antenna spacing, the sensor registering the highest maximum temperatures changed: The highest mean maximum temperatures were recorded by sensors B and C (101 °C) for 3-cm spacing, sensor C (88 °C) for 4-cm spacing, and sensors C and D (59 °C) for 5-cm spacing. During simultaneous ablation for 15 min, the mean maximum temperatures recorded by the peripheral sensors D and E were higher for 4 cm (79 °C and 58 °C) than for 3 cm (75 °C and 55 °C) or 5 cm (59 °C and 50 °C) antenna spacings, respectively. In the three simultaneous activation protocols resulting in confluent ablation zones (4-cm spacing for 15 min and 3-cm spacing for both 10 and 15 min; all using simultaneous power delivery), the mean temperatures recorded by Sensor A during the cooling periods declined more slowly than the mean temperatures recorded by Sensors B and C

tissue, whereas MWA energy does, potentially resulting in larger and more uniform ablation zones [8, 13, 24].

Based on these differences between RFA and MWA, we opted to use four antennas, antenna spacings of 3 cm and higher, and 60-W power in our study. The result showed the largest ablation zone occurred with antennas placed 4 cm (vs. 3 cm or 5 cm) apart. Moreover, at the same ablation settings, simultaneous ablation took a quarter of the time, created larger ablation zone diameters, and resulted in smaller CR than sequential ablation, which was similar to the result of Harari et al. [5].

It has been reported that the radius of single-antenna MWA zones was 1.5 cm under 60 W for 15 min [25]. Furthermore, synergistic effect may occur between the adjacent antennas when multiple antennas are applied together, resulting in increased thermal efficiency and

extension of the thermal field produced by each individual antenna [11]. Therefore, if we set antenna spacing at 3 cm (twice as the radius of single-antenna MWA) or even 4 cm, and performed simultaneous antenna activation for either 10 or 15 min, the resulting ablation shapes were confluent. Another result from the mean maximum temperatures proved that the temperatures at the ablation zones margin were highest at 4-cm antenna spacing (rather than 3 cm or 5 cm). Therefore, the finding that the largest ablation zones occurred with 4-cm antenna spacing could be attributable to the combination of synergistic effect between the antennas and the highest peripheral energy deposition.

Defining optimal multi-antenna spacing distances for MWA is likely to have substantial clinical significance, particularly when approaching the treatment of large HCC in humans. For example, if our findings from this ex vivo bovine model were even proportionally transferrable to in vivo human liver tissue, despite the cooling effect in in vivo liver with blood perfusion, it would be helpful to know that using simultaneous 4-antenna MWA at 60 watts for 15 min, a tumor less than 7 cm in diameter would probably be ablated with antennas spaced 4 cm apart.

Additionally, Amabile et al. and Farina et al. also described liver and muscle shrinkages in response to single-antenna MWA, attributing the phenomenon to dehydration effect [26, 27]. However, there was no study discussing ablation zone contraction of multi-antenna MWA. Using multi-antenna MWA, we found that the contraction ratio was significantly higher for simultaneous, longer duration, and narrower antenna spacing.

This study had some limitations. We fixed the power output and antenna number for all ablations, with only two ablation durations. Besides, we used an ex vivo bovine liver model without pathological examination and lacked active blood perfusion, therefore, so despite the fact that our findings may help further the understanding of the basic relationships between treatment variables and results in hepatic MWA, they may not all be directly transferrable to in vivo liver ablation in humans.

Conclusion

In the ex vivo bovine liver model, simultaneous 4-antenna MWA results in larger ablation zones than sequential MWA. Using 60-W power, simultaneous ablation with 4-cm antenna spacing and 15-minute ablation duration create a confluent ablation zone of 7.45 cm diameter. The *CR* may be useful as an aid to describing and comparing ablation zone shapes. This information may provide multi-antenna MWA strategies for large HCC in the further clinical practice.

Acknowledgements We would like to thank Ms. Xin Zheng for providing support and encouragement to Dr. Tianqi Zhang on his scientific research work.

Author Contributions Tian-Qi Zhang and Sen-Miao Huang participated equally in experiments and analyzed the data; Zhi-Mei Huang and Han-Xia Deng finished the statistical analysis; Tian-Qi Zhang finished the manuscript drafting; Yang-Kui Gu and Xiong-Ying Jiang gave the critical revision of the manuscript for important intellectual content; Jin-Hua Huang designed and coordinated the research.

Funding This work was supported by National Natural Science Foundation of China (No. 81771955), Guangzhou Science and Technology Program, key projects of collaborative innovation of health medicine (No. 201704020228), and Guangzhou Science and Technology Program, key projects of collaborative innovation of production, learning and research (No. 201704020134), Sun Yat-sen University Clinical Trial 5010 Project (No. 2016002).

Compliance with Ethical Standards

Conflict of interest The authors declare that they have no conflict of interest.

Ethical Approval All procedures performed in studies involving animals were in accordance with the ethical standards of the institution or practice at which the studies were conducted.

Informed Consent For this type of study, informed consent is not required.

References

1. Kim YS, Lim HK, Rhim H, Lee MW. Ablation of hepatocellular carcinoma. Best Pract Res Clin Gastroenterol. 2014;28(5):897–908.
2. Bruix J, Reig M, Sherman M. Evidence-based diagnosis, staging, and treatment of patients with hepatocellular carcinoma. Gastroenterology. 2016;150(4):835–53.
3. Xu Y, Shen Q, Wang N, Liu P, Wu P, Peng Z, et al. Percutaneous microwave ablation of 5-6 cm unresectable hepatocellular carcinoma: local efficacy and long-term outcomes. Int J Hyperthermia. 2016;9:1–8.
4. Dou JPLP, Yu J. Microwave ablation for liver tumors. Abdom Radiol (NY). 2016;41(4):650–8.
5. Harari CM, Magagna M, Bedoya M, Lee FT Jr, Lubner MG, Hinshaw JL, et al. Microwave ablation: comparison of simultaneous and sequential activation of multiple antennas in liver model systems. Radiology. 2016;278(1):95–103.
6. Chen MH, Yang W, Yan K, Zou MW, Solbiati L, Liu JB, et al. Large liver tumors: protocol for radiofrequency ablation and its clinical application in 110 patients—mathematic model, overlapping mode, and electrode placement process. Radiology. 2004;232(1):260–71.
7. Goldberg SN, Solbiati L, Hahn PF, Cosman E, Conrad JE, Fogle R, et al. Large-volume tissue ablation with radio frequency by using a clustered, internally cooled electrode technique: laboratory and clinical experience in liver metastases. Radiology. 1998;209(2):371–9.
8. Haemmerich D, Lee FT Jr, Schutt DJ, Sampson LA, Webster JG, Fine JP, et al. Large-volume radiofrequency ablation of ex vivo bovine liver with multiple cooled cluster electrodes. Radiology. 2005;234(2):563–8.

9. Choi TW, Lee JM, Lee DH, Lee JH, Yu SJ, Kim YJ, et al. Percutaneous dual-switching monopolar radiofrequency ablation using a separable clustered electrode: a preliminary study. Korean J Radiol. 2017;18(5):799–808.
10. Yoon JH, Lee JM, Hwang EJ, Hwang IP, Baek J, Han JK, et al. Monopolar radiofrequency ablation using a dual-switching system and a separable clustered electrode: evaluation of the in vivo efficiency. Korean J Radiol. 2014;15(2):235–44.
11. Brace CL, Laeseke PF, Sampson LA, Frey TM, van der Weide DW, Lee FT Jr. Microwave ablation with multiple simultaneously powered small-gauge triaxial antennas: results from an in vivo swine liver model. Radiology. 2007;244(1):151–6.
12. Oshima F, Yamakado K, Nakatsuka A, Takaki H, Makita M, Takeda K. Simultaneous microwave ablation using multiple antennas in explanted bovine livers: relationship between ablative zone and antenna. Radiat Med. 2008;26(7):408–14.
13. Wright AS, Lee FT Jr, Mahvi DM. Hepatic microwave ablation with multiple antennae results in synergistically larger zones of coagulation necrosis. Ann Surg Oncol. 2003;10(3):275–83.
14. Simon CJ, Dupuy DE, Iannitti DA, Lu DS, Yu NC, Aswad BI, et al. Intraoperative triple antenna hepatic microwave ablation. AJR Am J Roentgenol. 2006;187(4):W333–40.
15. Yu NC, Lu DS, Raman SS, Dupuy DE, Simon CJ, Lassman C, et al. Hepatocellular carcinoma: microwave ablation with multiple straight and loop antenna clusters—pilot comparison with pathologic findings. Radiology. 2006;239(1):269–75.
16. Farina L, Weiss N, Nissenbaum Y, Cavagnaro M, Lopresto V, Pinto R, et al. Characterisation of tissue shrinkage during microwave thermal ablation. Int J Hyperthermia. 2014;30(7):419–28.
17. Ren H, An C, Liang P, Yu J, Cheng Z, Han Z, et al. Ultrasound-guided percutaneous microwave ablation assisted by a three-dimensional visualization treatment platform combined with transcatheter arterial chemoembolization for a single large hepatocellular carcinoma 5 cm or larger: a preliminary clinical application. Int J Hyperthermia. 2018. https://doi.org/10.1080/02656736.2018.1530459.
18. Kang TW, Lim HK, Cha DI. Percutaneous ablation for perivascular hepatocellular carcinoma: refining the current status based on emerging evidence and future perspectives. World J Gastroenterol. 2018;24(47):5331–7.
19. Dou JP, Yu J, Yang XH, Cheng ZG, Han ZY, Liu FY, et al. Outcomes of microwave ablation for hepatocellular carcinoma adjacent to large vessels: a propensity score analysis. Oncotarget. 2017;8(17):28758–68.
20. Jiang C, Liu B, Chen S, Peng Z, Xie X, Kuang M. Safety margin after radiofrequency ablation of hepatocellular carcinoma: precise assessment with a three-dimensional reconstruction technique using CT imaging. Int J Hyperthermia. 2018;34(8):1135–41.
21. Adeyanju OO, Al-Angari HM, Sahakian AV. The optimization of needle electrode number and placement for irreversible electroporation of hepatocellular carcinoma. Radiol Oncol. 2012;46(2):126–35.
22. Sakakibara M, Ohkawa K, Imanaka K, Miyazaki M, Nawa T, Kimura H, et al. Quick and stable parallel puncture of hepatic tumors using a double-barreled needle direction system for ultrasound-guided bipolar radiofrequency ablation. Hepatol Res. 2016;46(11):1152–7.
23. Mulier S, Jiang Y, Wang C, Jamart J, Marchal G, Michel L, et al. Bipolar radiofrequency ablation with four electrodes: ex vivo liver experiments and finite element method analysis. Influence of inter-electrode distance on coagulation size and geometry. Int J Hyperthermia. 2012;28(7):686–97.
24. Brace CL, Sampson LA, Hinshaw JL, Sandhu N, Lee FT Jr. Radiofrequency ablation: simultaneous application of multiple electrodes via switching creates larger, more confluent ablations than sequential application in a large animal model. J Vasc Interv Radiol. 2009;20(1):118–24.
25. Amabile C, Ahmed M, Solbiati L, Meloni MF, Solbiati M, Cassarino S, et al. Microwave ablation of primary and secondary liver tumours: ex vivo, in vivo, and clinical characterisation. Int J Hyperthermia. 2017;33(1):34–42.
26. Amabile C, Farina L, Lopresto V, Pinto R, Cassarino S, Tosoratti N, et al. Tissue shrinkage in microwave ablation of liver: an ex vivo predictive model. Int J Hyperthermia. 2017;33(1):101–9.
27. Farina L, Nissenbaum Y, Cavagnaro M. Tissue shrinkage in microwave thermal ablation: comparison of three commercial devices. Int J Hyperthermia. 2017;16:1–10.